4. Transition Path Theory for Markov Jump Processes

Continuous-time Markov chains on discrete state-space have an enormous range of applications. In recent years, especially, with the explosion of new applications in network science, Markov chains have become the tool of choice not only to model the dynamics on these networks but also to study their topological properties [2, 68]. In this context, there is a need for new methods to analyze Markov chains on large state-space with no specific symmetries, as relevant for large complex networks.

A natural starting point to analyze a Markov chain is to use spectral analysis. This is especially relevant when the chain displays metastability, as was shown in [12, 24] in the context of time-reversible chains. By definition, the generator of a metastable chain possesses one or more clusters of eigenvalues near zero, and the associated eigenvectors provide a natural way to partition the chain (and hence the underlying network) in cluster of nodes on which the walker remains for a very long time before finding its way to another such cluster. This approach has been used not only in the context of Markov chains arising from statistical physics (such as e.g. glassy systems [4, 11] or bio-molecules [81]), but also in the context of data segmentation and embedding [84, 62, 78, 6, 26, 16, 55]. The problem with the spectral approach, however, is that not all Markov chains of interest are time-reversible and metastable, and when they are not, the meaning of the first few eigenvectors of the generator is less clear.

In this chapter, we take another approach which does not require metastability and applies for non-time-reversible chains as well. The basic idea is to single out two disjoint subsets of nodes of interest in the state-space of the chain and ask what is the typical mechanism by which the walker transits from one of these subsets to the other? We can also ask what is the rate at which these transitions occur, etc. The first object which comes to mind to characterize these transitions is the path of maximum likelihood by which they occur. However, this path can again be not very informative with respect to its relevance for the transition process. For an attempt to characterize transition pathways by means of the likelihood by which they occur see Chapter 6.

The main objective of this chapter, however, is to adapt the framework of transition path theory (TPT) on discrete state space which allows to give a precise meaning to the question of finding typical the mechanism and rate of transition even in chains which are neither metastable nor time-reversible. We will focus only on continuous-time Markov chains, but we note that the results can be straightforwardly extended to the case of discrete-time Markov chains.

Besides the illustration of the output of the theory on a test example, we will apply discrete TPT in order to study the conformational dynamics of the bio-molecule glycine as well as the dynamics of a genetic toggle switch model.

We want to point out that tools of TPT presented here can be used for data

segmentation as well. In this context, TPT provides an alternative to Laplacian eigenmaps [78, 6] and diffusion maps [16] which have become very popular recently in data analysis. In this thesis, we will not, however, develop these ideas any further.

4.1. Theoretical Aspects

4.1.1. Preliminaries: Notations and Assumptions

We will consider a Markov jump process on the countable state-space S with infinitesimal generator (or rate matrix) $L = (l_{ij})_{i,j\in S}$:

$$\begin{cases} l_{ij} \geq 0 & \text{for all } i,j \in S, i \neq j \\ \sum_{j\in S} l_{ij} = 0 & \text{for all } i \in S. \end{cases}$$

as introduced in Section 2.2. We assume that this process is irreducible and ergodic with respect to the unique, strictly positive stationary distribution $\pi = (\pi_i)_{i\in S}$. We will denote by $\{X(t)\}_{t\in\mathbb{R}}$ an equilibrium sample path (or trajectory) of the Markov jump process, i.e. any path obtained from $\{X(t)\}_{t\in[T,\infty)}$ by pushing back the initial condition, $X(T) = x$, at $T = -\infty$. Throughout that chapter, we do not assume reversibility.

For the algorithmic part of this chapter, it will be convenient to use the notations and concepts of Graph Theory. We will mainly consider directed graphs $G = G(S, E)$ where the vertex set S is the set of all states of the Markov jump process and two vertices i and j are connected by a *directed edge* if $(i, j) \in E \subseteq (S \times S)$. Let $E' \subset E$ be a subset of edges of a graph $G = G(S, E)$, then we denote by $G(S', E')$ the *induced subgraph*, i.e. the graph which consists of all edges in E' and the vertex set

$$S' = \{i \in S : \exists j \in S \text{ s.t. } (i, j) \in E' \text{ or } (j, i) \in E'\}.$$

We also recall that:

Definition 4.1.1. *A* directed pathway $w = (i_0, i_2, \ldots, i_n),\ i_j \in S, j = 0, \ldots, n$ *in a graph G is a finite sequence of vertices such that $(i_j, i_{j+1}) \in E, j = 0, \ldots, n-1$. A directed pathway w is called* simple *if w does not contain any self-intersections (loops), i.e. $i_j \neq i_k$ for $j, k \in \{0, \ldots, n\}, j \neq k$.*

We will later consider several forms of weight-induced directed graphs:

Definition 4.1.2. *Whenever a $|S| \times |S|$-matrix $C = (C_{ij})$ with non-negative entries is given, the* weight-induced directed graph *is denoted by $G\{C\} = G(S, E)$. In this graph the vertex set S is the set of all states of the Markov jump process and two vertices i and j are connected by a* directed edge $(i, j) \in E \subseteq (S \times S)$ *if the corresponding* weight C_{ij} *is positive.*

4.1.2. Reactive Trajectories

Let A and B be two nonempty, disjoint subsets of the state space S. By ergodicity, any equilibrium path $\{X(t)\}_{t\in\mathbb{R}}$ oscillates infinitely many times between set A and set B. We are interested in understanding how these oscillations happen (mechanism, rate, etc). If we view A as a reactant state and B as a product state, each oscillation

from A to B is a reaction event, and so we are asking about the mechanism, rate, etc. of these reaction events. To properly define and characterize the reaction events, we proceed by pruning a long ergodic trajectory $\{X(t)\}_{t\in\mathbb{R}}$ into pieces during which it makes a transition from A to B, and ask about various statistical properties of these pieces, see Fig. 4.1. The pruning is done as follows.

First, given a trajectory $\{X(t)\}_{t\in\mathbb{R}}$ we define a set of exit and entrance times $\sigma = \{t_n^A, t_n^B\}_{n\in\mathbb{Z}}$ as:

Definition 4.1.3 (Exit and entrance times)**.** *Given a trajectory $\{X(t)\}_{t\in\mathbb{R}}$, the exit time t_n^A and the entrance time t_n^B belong to σ if and only if*

$$\begin{gathered}\lim_{t\to t_n^A-} X(t) = x_n^A \in A, \quad X(t_n^B) = x_n^B \in B,\\ \forall t \in [t_n^A, t_n^B) : X(t) \notin A \cup B.\end{gathered} \tag{4.1}$$

By ergodicity, we know that the cardinal of σ is infinite. It is also clear that the times t_n^A and t_n^B form an increasing sequence, $t_n^A \le t_n^B \le t_{n+1}^A$ for all $n \in \mathbb{Z}$. Notice however that we may have $t_n^A = t_n^B$ for some $n \in \mathbb{Z}$ corresponding to events when the trajectory jumps directly from A to B. If, on the other hand, $t_n^A < t_n^B$, then the trajectory visits states outside of A and B when it makes a transition from the former to the latter.

Next, given the set σ, we define:

Definition 4.1.4 (Reactive times)**.** *The set R of reactive times is defined as*

$$R = \bigcup_{n\in\mathbb{Z}} (t_n^A, t_n^B) \subset \mathbb{R}. \tag{4.2}$$

Finally, we denote by $t_n^1 \equiv t_n^A \le t_n^2 \le \cdots \le t_n^{k_n} \le t_n^B$ the set of all the successive jumping times of $X(t)$ in $[t_n^A, t_n^B]$, i.e. all the times in $[t_n^A, t_n^B]$ such that

$$\lim_{t\to t_n^k-} X(t) \neq X(t_n^k) =: x_n^k, \qquad k = 1, \ldots, k_n \in \mathbb{N} \tag{4.3}$$

and we define:

Definition 4.1.5 (Reactive trajectories)**.** *The ordered sequence*

$$P_n = [x_n^A, x_n^1, x_n^2 \ldots, x_n^{k_n} \equiv x_n^B]$$

consisting of the successive states visited during the n^{th} transition from A to B (including the last state in A, x_n^A, and the first one in B, $x_n^B \equiv x_n^{k_n}$) is called the n^{th} reactive trajectory. The set of all such sequences,

$$P = \bigcup_{n\in\mathbb{Z}} \{P_n\} \tag{4.4}$$

is called the set of reactive trajectories.

(Note that we have $k_n = 1$ when the trajectory hops directly from A to B at time $t_n^A = t_n^B$, in which case $P_n = [x_n^A, x_n^B]$.)

In the next sections we obtain various statistical properties of the objects defined in this section. Note that, because of the way we defined these objects they do depend on the particular trajectory $\{X(t)\}_{t\in\mathbb{R}}$ used to generate them. However, their law does not.

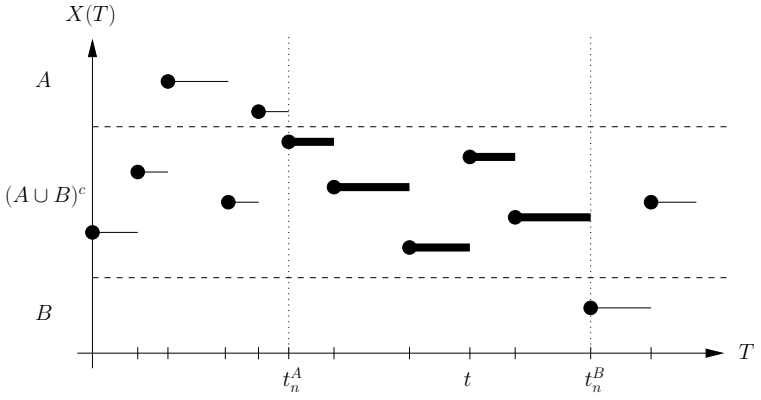

Figure 4.1.: Schematic representation of a piece of an ergodic trajectory. The subpiece connecting A to B (shown in thick black) is a reactive trajectory, and the collection of reactive trajectories is the ensemble of reactive trajectories.

4.1.3. Probability Distribution of Reactive Trajectories

A first object relevant to quantify the statistical properties of the reactive trajectories is:

Definition 4.1.6. *The distribution of reactive trajectories $m^R = (m_i^R)_{i\in S}$ is defined so that for any $i \in S$ we have:*

$$\lim_{T\to\infty} \frac{1}{2T} \int_{-T}^{T} \mathbf{1}_{\{i\}}(X(t))\mathbf{1}_R(t)\,dt = m_i^R, \tag{4.5}$$

where $\mathbf{1}_C(\cdot)$ denotes the characteristic function of the set C.

The distribution m^R gives the equilibrium probability to observe a reactive trajectory at state i and time t.

How can we find an expression for m^R? Suppose we encounter the process $X(t)$ in a state $i \in S$. What is the probability that $X(t)$ be reactive? Intuitively, this is the probability that the process came rather from A than from B times the probability that the process will reach B rather than A in the future. This indicates that the following objects will play an important role:

Definition 4.1.7. *The discrete forward committor $q^+ = (q_i^+)_{i\in S}$ is defined as the probability that the process starting in $i \in S$ will reach first B rather than A. Analogously, we define the discrete backward committor $q^- = (q_i^-)_{i\in S}$ as the probability that the process arriving in state i came last from A rather than B.*

In the next section we show that the forward and backward committor satisfy a discrete Dirichlet problem, respectively.

We have

Theorem 4.1.1. *The probability distribution of reactive trajectories defined in (4.5) is given by*

$$m_i^R = \pi_i q_i^+ q_i^-, \quad i \in S. \tag{4.6}$$

Proof. Denote by $x_i^{AB,+}(t)$ the first state in $A \cup B$ reached by $X(s)$, $s \geq t$, conditional on $X(t) = i$. Similarly, denote by $x_i^{AB,-}(t)$ the last state in $A \cup B$ left by $X(s)$, $s \leq t$, conditional on $X(t) = i$ or, equivalently, the first state in $A \cup B$ reached by $X^R(s)$, $s \geq -t$. In terms of these quantities, (4.5) can be written as

$$m_i^R = \lim_{T \to \infty} \frac{1}{2T} \int_{-T}^{T} \mathbf{1}_{\{i\}}(X(t)) \mathbf{1}_A(x_i^{AB,-}(t)) \mathbf{1}_B(x_i^{AB,+}(t)) \mathrm{d}t.$$

Taking the limit as $T \to \infty$ and using ergodicity together with the strong Markov property, we deduce that

$$m_i^R = \pi_i \, \mathbb{P}_i(\tau_B^+ < \tau_A^+) \mathbb{P}_i^R(\tau_B^- > \tau_A^-)$$

which is (4.6) by definition of q^+ and q^-. □

Notice that $m_i^R = 0$ if $i \in A \cup B$. Notice also that m^R is not a normalized distribution. In fact,

$$Z_{AB} = \sum_{j \in S} m_j^R = \sum_{j \in S} \pi_j q_j^+ q_j^- \leq 1$$

is the probability that the trajectory is reactive at some given instance t in time, i.e.

$$Z_{AB} = \mathbb{P}(t \in R). \tag{4.7}$$

The distribution

$$m_i^{AB} = Z_{AB}^{-1} m_i^R = Z_{AB}^{-1} \pi_i q_i^+ q_i^- \tag{4.8}$$

is then the normalized distribution of reactive trajectories which gives the probability to observe a reactive trajectory at state i at time t conditional on the trajectory being reactive at time t.

Remark 4.1.8. *If the Markov process is reversible (i.e. $\pi_i l_{ij} = \pi_j l_{ji}$), then $q_i^+ = 1 - q_i^-$ and the probability distribution of reactive trajectories reduces to*

$$m_i^R = \pi_i q_i^+ (1 - q_i^+) \qquad \textit{(reversible process).} \tag{4.9}$$

4.1.4. Discrete Committor Equations

The discrete forward and backward committors play a central role in TPT. Recall, that for a state $i \in S$ the discrete forward committor q_i^+ is defined as the probability that the Markov jump process starting in state i will reach B rather than A. In other words, q_i^+ is the first entrance probability of the process $\{X(t), t \geq 0, X(0) = i\})$ with respect to the set B *avoiding* the set A. The usual step in dealing with entrance or hitting probabilities with respect to a certain subset of states is the modification of the process such that these states become *absorbing* states. Let $L = (l_{ij})_{i,j \in S}$ be the infinitesimal generator of a Markov jump process and $A \subset S$ be a non-empty subset. Suppose we are interested in the process resulting from the declaration of the states in A to be absorbing states. Then the infinitesimal generator $\hat{L} = (\hat{l}_{ij})_{i,j \in S}$ of the modified process is given by, [89]

$$\hat{l}_{ij} = \begin{cases} l_{ij} & i \in A^c, j \in S \\ 0 & i \in A, j \in S \end{cases} \tag{4.10}$$

From this viewpoint, now it is simple to prove the following theorem.

Theorem 4.1.2. *Let q_i^+ be the probability to reach B before A provided that the process has started in state $i \in S$. Then the discrete forward committor $q^+ = (q_i^+)_{i\in S}$ satisfies the equations*

$$\begin{cases} \sum_{k\in S} l_{ik} q_k^+ = 0, & \forall i \in (A \cup B)^c \\ q_i^+ = 0, & \forall i \in A \\ q_i^+ = 1, & \forall i \in B \end{cases} \tag{4.11}$$

Proof. If we make the states in the set A absorbing states then the discrete forward committor q^+ is the first entrance probability with respect to the set B under the modified process. Thus q^+ satisfies the discrete Dirichlet problem [89]

$$\begin{cases} \sum_{k\in S} \hat{l}_{ik} q_k^+ & = 0, \quad \forall i \in B^c \\ q_i^+ & = 1, \quad \forall i \in B \end{cases}$$

or, equivalently,

$$\begin{cases} \sum_{k\in S} l_{ik} q_k^+ = 0, & \forall i \in (A \cup B)^c \\ q_i^+ = 0, & \forall i \in A \\ q_i^+ = 1, & \forall i \in B \end{cases}$$

which ends the proof. □

Observe that if we substitute the "boundary conditions" into the equations in (4.11) we end up with a linear system

$$Uq^+ = v, \tag{4.12}$$

where the matrix $U = (u_{ij})_{i,j\in(A\cup B)^c}$ is given by

$$u_{ij} = l_{ij} \quad i, j \in (A \cup B)^c$$

and an entry of the vector $v = (v_i)_{i\in(A\cup B)^c}$ on the right hand side of (4.12) is defined by $v_i = -\sum_{k\in B} l_{ik}, \forall i \in (A \cup B)^c$. Now we can prove

Lemma 4.1.9. *If the matrix U is irreducible then the solution of (4.11) is unique.*

Proof. By the definition of the matrix U there exists at least an index $k \in (A \cup B)^c$ such that

$$|u_{kk}| > \sum_{j\neq k} u_{kj}.$$

But this implies that U is weakly diagonally dominant (see Definition A.58). Together with its assumed irreducibility, Theorem A.6.6 in the Appendix implies that it is invertible. □

Next, we turn our attention to the discrete backward committor $q_i^-, i \in S$ which is defined as the probability that the process arriving at state i came rather from A than from B. The crucial observation is now that $q^- = (q_i^-)_{i\in S}$ is the discrete forward committor with respect to the *reversed time process*.

Theorem 4.1.3. *The discrete backward committor $q^- = (q_i^-)_{i\in S}$ satisfies the linear system of equations*

$$\begin{cases} \sum_{k\in S} l_{ik}^R q_k^- = 0, & \forall i \in (A\cup B)^c \\ q_i^- = 1, & \forall i \in A \\ q_i^- = 0, & \forall i \in B, \end{cases} \tag{4.13}$$

where $\pi = (\pi_i)_{i\in S}$ is a stationary distribution and $l_{ik}^R = \pi_k l_{ki}/\pi_i$ is the generator of the reversed time process (see (2.49)). Moreover, if the Markov jump process is reversible then the backward committor is simply related to the forward committor by

$$q^- = 1 - q^+. \tag{4.14}$$

Proof. The derivation of (4.13) is a straightforward generalization of the one of (4.11). To derive (4.14), note that if the Markov jump process is reversible, then the detailed balance 2.50 condition is satisfied and the discrete backward committor solves

$$\begin{cases} \sum_{k\in S} l_{ik} q_k^- = 0, & \forall i \in (A\cup B)^c \\ q_i^- = 1, & \forall i \in A \\ q_i^- = 0, & \forall i \in B. \end{cases} \tag{4.15}$$

On one hand the solution of the discrete Dirichlet problem (4.15) is unique (see Lemma 4.1.9). On the other hand, a short calculation shows that $1-q^+$ also satisfies (4.15). Consequently, we have $q^- = 1 - q^+$ which ends the proof. □

Remark 4.1.10. *The committor q_i^+ is related to hitting times with respect to the sets A and B by*

$$q_i^+ = \mathbb{P}_i(\tau_B^+ < \tau_A^+). \tag{4.16}$$

Here $\mathbb{P}_i$ denotes expectation conditional on $X(0) = i$, $\tau_A^+ = inf\{t > 0 : X(t) \in A\}$ denotes the first entrance time of the set A and $\tau_B^+ = inf\{t > 0 : X(t) \in B\}$ the first entrance time of the set B; q_i^- can be defined similarly using the time-reversed process as

$$q_i^- = \mathbb{P}^R{}_i(\tau_B^- > \tau_A^-), \tag{4.17}$$

where $\mathbb{P}^R{}_i$ denotes expectation with respect to the time-reversed process conditional on $X^R(0) = i$, $\tau_A^- = inf\{t > 0 : X^R(t) \in A\}$ denotes the last exit time of the subset A and $\tau_B^- = inf\{t > 0 : X^R(t) \in B\}$ the last exit time of the subset B.

4.1.5. Probability Current of Reactive Trajectories

In this section we are interested in the average current of reactive trajectories flowing from state i to state j per time unit. More precisely:

Definition 4.1.11. *The probability current of reactive trajectories $f^{AB} = (f_{ij}^{AB})_{i,j\in S}$ is defined so that for all pairs of states $(i,j), i,j \in S, i \neq j$ we have*

$$\begin{aligned} \lim_{s\to 0+} \frac{1}{s} \lim_{T\to\infty} \frac{1}{2T} \int_{-T}^{T} \mathbf{1}_{\{i\}}(X(t)) \mathbf{1}_{\{j\}}(X(t+s)) \\ \times \sum_{n\in\mathbb{Z}} \mathbf{1}_{(-\infty, t_n^B]}(t) \mathbf{1}_{[t_n^A,\infty)}(t+s)\, dt = f_{ij}^{AB}. \end{aligned} \tag{4.18}$$

In addition, we set $f_{ii}^{AB} = 0$ for all $i \in S$.

We have

Theorem 4.1.4. *The discrete probability current of reactive trajectories is given by*

$$f_{ij}^{AB} = \begin{cases} \pi_i q_i^- l_{ij} q_j^+, & \text{if } i \neq j \\ 0, & \text{otherwise} \end{cases} \tag{4.19}$$

Proof. Using the same notations as in the proof of Theorem 4.1.1, equation (4.18) can also be written as

$$\begin{aligned} f_{ij}^{AB} = \lim_{s\to 0^+} \frac{1}{s} \lim_{T\to\infty} \frac{1}{2T} \int_{-T}^{T} & \mathbf{1}_{\{i\}}(X(t)) \mathbf{1}_{\{j\}}(X(t+s)) \\ & \times \mathbf{1}_A(x_i^{AB,-}(t)) \mathbf{1}_B(x_j^{AB,+}(t+s)) \mathrm{d}t. \end{aligned} \tag{4.20}$$

Taking the limit $T \to \infty$ and using ergodicity, we deduce that

$$f_{ij}^{AB} = \lim_{s\to 0^+} \frac{1}{s} \pi_i q_i^- \mathbb{E}_i[q_{X(s)}^+, \mathbf{1}_{\{j\}}(X(s))],$$

where $\mathbb{E}_i$ denotes the expectation conditional on $X(0) = i$. To take the limit $s \to 0^+$ we use

$$\forall \Phi : S \mapsto \mathbb{R} : \lim_{s\to 0^+} \frac{1}{s} (\mathbb{E}_i[\Phi(X(s))] - \Phi(i)) = \sum_{j\in S} l_{ij} \Phi(j)$$

and we are done since $i \neq j$. □

This result implies an expected property, the conservation of the discrete probability current or flux in each node:

Theorem 4.1.5. *For all $i \in (A \cup B)^c$ the probability current is conserved, i.e.*

$$\sum_{j\in S} (f_{ij}^{AB} - f_{ji}^{AB}) = 0, \quad \forall i \in (A \cup B)^c. \tag{4.21}$$

Proof. By definition of f^{AB} for $i \in (A \cup B)^c$:

$$\begin{aligned} \sum_{j\in S} (f_{ij}^{AB} - f_{ji}^{AB}) &= \pi_i q_i^- \sum_{j\neq i} l_{ij} q_j^+ - \pi_i q_i^+ \sum_{j\neq i} \frac{\pi_j}{\pi_i} l_{ji} q_j^- \\ &= -q_i^- q_i^+ \pi_i l_{ii} + q_i^- q_i^+ \pi_i l_{ii}^R = 0, \end{aligned}$$

where we used $\sum_{j\in S} l_{ij} q_j^+ = 0$ if $i \in (A \cup B)^c$ from (4.11) and $\sum_{j\in S} l_{ij}^R q_j^- = 0$ if $i \in (A \cup B)^c$ from (4.15). □

For later use we should also mention that conservation of the current in every state $i \in (A \cup B)^c$ immediately implies the following total conservation of the current,

$$\sum_{i\in A, j\in S} f_{ij}^{AB} = \sum_{j\in S, i\in B} f_{ji}^{AB}, \tag{4.22}$$

where we used that $f_{ij}^{AB} = 0$ if $i \in S$ and $j \in A$, and $f_{ij}^{AB} = 0$ if $i \in B$ and $j \in S$.

4.1.6. Transition Rate and Effective Current

In this section we derive the average number of transitions from A to B per time unit or, equivalently, the average number of reactive trajectories observed per time unit. More precisely, let $N_T^-, N_T^+ \in \mathbb{Z}$ be such that

$$R \cap [-T, T] = \bigcup_{N_T^- \le n \le N_T^+} (t_n^A, t_n^B), \tag{4.23}$$

that is, $N_T^+ - N_T^-$ is the number of reactive trajectories in the interval $[-T, T]$ in time.

Then:

Definition 4.1.12. *The transition (reaction) rate k_{AB} is defined as*

$$k_{AB} = \lim_{T\to\infty} \frac{N_T^+ - N_T^-}{2T}. \tag{4.24}$$

We have:

Theorem 4.1.6. *The transition rate is given by*

$$k_{AB} = \sum_{i\in A, j\in S} f_{ij}^{AB} = \sum_{j\in S, k\in B} f_{jk}^{AB}. \tag{4.25}$$

Proof. From (4.20) we get

$$\sum_{i\in A, j\in S} f_{ij}^{AB} = \lim_{s\to 0^+} \frac{1}{s} \lim_{T\to\infty} \frac{1}{2T} \times \int_{-T}^{T} \mathbf{1}_A(X(t)) \sum_{j\in S} \mathbf{1}_B(x_j^{AB,+}(t+s))\mathrm{d}t. \tag{4.26}$$

Let us consider the integral; we can always restrict our attention to generic values of T such that there is no $n \in \mathbb{Z}$ for which $T = t_n^A$ or $T = t_n^B$. The integrand in this expression is nonzero *iff* $X(t) \in A$, $X(t+s) \in A^c$ and $t+s \in R$, i.e. if $t_n^A \in (t, t+s)$ for some $n \in \mathbb{Z}$. But this means that the integral of $\mathbf{1}_A(X(t))\mathbf{1}_B(x_j^{AB,+}(t+s))$ on every interval $t \in (t_n^A - s, t_n^A)$ is equal to s and the only contributions to the integral in (4.26) come from the intervals in $[-T, T] \cap \cup_{n\in\mathbb{Z}}(t_n^A - s, t_n^A)$. But these are exactly $N_T^+ - N_T^-$ intervals such that the whole integral amounts to $(N_T^+ - N_T^-)s$. From (4.26) and (4.23), this implies the first identity for the rate k_{AB}. The second identity follows from (4.22). □

Notice that the rate can also be expressed as

$$k_{AB} = \sum_{i\in A, j\in S} f_{ij}^+, \tag{4.27}$$

where:

Definition 4.1.13. *The effective current is defined as*

$$f_{ij}^+ = \max(f_{ij}^{AB} - f_{ji}^{AB}, 0). \tag{4.28}$$

Identity (4.27) follows from (4.25) and the fact that $\forall i \in A : f_{ij}^{+} = f_{ij}^{AB}$ since $f_{ji}^{AB} = 0$ and $f_{ij}^{AB} > 0$ if $i \in A$. The effective current gives the net average number of reactive trajectories per time unit making a transition from i to j on their way from A to B. The effective current will be useful to define transition pathways in Section 4.1.8.

Remark 4.1.14. *If the Markov process is reversible, then the effective current reduces to*

$$f_{ij}^{+} = \begin{cases} \pi_i l_{ij}(q_j^{+} - q_i^{+}), & \text{if } q_j^{+} > q_i^{+} \\ 0, & \text{otherwise} \end{cases} \qquad \text{(reversible process)} \tag{4.29}$$

and the reaction rate can be expressed as

$$k_{AB} = \tfrac{1}{2} \sum_{i,j \in S} \pi_i l_{ij}(q_j^{+} - q_i^{+})^2. \qquad \text{(reversible process)} \tag{4.30}$$

The last identity can also be written as $k_{AB} = -\sum_{i \in S, j \in B} \pi_i l_{ij} q_i^{+}$ *(for reversible processes!) which in turn is identical to the expression that we know from Theorem 4.1.6*

$$k_{AB} = \sum_{\substack{i \in S, j \in B \\ i \neq j}} \pi_i l_{ij}(1 - q_i^{+}). \qquad \text{(reversible process)}$$

4.1.7. Relations with Electrical Resistor Networks

Before proceeding further, it is interesting to revisit our result in the context of electrical resistor networks [27]. Recall that an *electrical resistor network* is a directed weighted graph $G(S, E) = G\{C\}$ where $C = (c_{ij})$ is an entry-wise nonnegative symmetric matrix (cf. Def. 4.1.2), called *conductance matrix* of G. The reciprocal r_{ij} of the conductance c_{ij} is called the *resistance* of the edge (i, j). Establishing a voltage $v_a = 0$ and $v_b = 1$ between two vertices a and b induces a voltage $v = (v_i)_{i \in S \setminus \{a,b\}}$ and an electrical current F_{ij} which are related by Ohm's Law

$$F_{ij} = \frac{v_i - v_j}{r_{ij}} = (v_i - v_j)c_{ij}, \ i, j \in S, i \neq j. \tag{4.31}$$

Furthermore, the Kirchhoff's Current Law, that is

$$\sum_{j \in S} F_{ij} = 0 \quad \forall i \in S \setminus \{a, b\} \tag{4.32}$$

requires that the voltages have the property

$$v_i = \sum_{j \neq i} \frac{c_{ij}}{c_i} v_j, \quad \forall i \in, S \setminus \{a, b\}, \tag{4.33}$$

where $c_i = \sum_{j \in S} c_{ij}$. A *reversible* Markov jump process, given by its infinitesimal generator L, can be seen as an electrical resistor network by setting up the conductance matrix C via

$$c_{ij} = \pi_i l_{ij},$$

where $\pi = (\pi_i)_{i\in S}$ is the unique stationary distribution. Now observe that equation (4.33) reduces to

$$0 = \sum_{j\in S} l_{ij} v_j, \quad \forall i \in S \setminus \{a, b\}.$$

But this means that the forward committor q^+ with respect to the sets $A = \{a\}$ and $B = \{b\}$ can be interpreted as a voltage. Moreover, a short calculation shows that the effective flux, defined in (4.28), pertains to the electrical current.

4.1.8. Dynamical Bottlenecks and Reaction Pathways

The transition rate k_{AB} is a quantity which is important to describe the global transition behavior. In this section we characterize the local *bottlenecks* of the ensemble of reactive trajectories which determine the transition rate. In order to get a detailed insight into the local transition behavior we characterize reaction pathways by looking on the amount of reactive trajectories which is conducted from A to B by a sequence of states.

We use the notations of Graph Theory introduced at the end of Section 4.1.1. Let $G(S, E) = G\{f^+\}$ be the weight induced directed graph associated with the effective current $f^+ = (f_{ij}^+),\ i_j \in S$. A simple pathway in the graph G, starting in $A \subset S$ and ending in $B \subset S$, is the natural choice for representing a specific reaction from A to B because any loop during a transition would be redundant with respect to the progress of the reaction.

Definition 4.1.15. *A* reaction pathway $w = (i_0, i_1, \ldots, i_n),\ i_j \in S, j = 0, \ldots, n$ *from A to B is a simple pathway such that*

$$i_0 \in A, i_n \in B, i_j \in (A \cup B)^c \quad j = 1, \ldots, n-1.$$

The crucial observation which leads to a characterization of bottlenecks of reaction pathways is that the amount of reactive trajectories which can be conducted by a reaction pathway per time unit is confined by the minimal effective current of a transition involved along the reaction pathway.

Definition 4.1.16. *Let $w = (i_0, i_1, \ldots, i_n)$ be a reaction pathway in $G\{f^+\}$. We define the* min-current *of w by*

$$c(w) = \min_{e=(i,j)\in w} \{f_{ij}^+\}. \tag{4.34}$$

The dynamical bottleneck *of a reaction pathway is the edge with the minimal effective current*

$$(b_1, b_2) = arg \min_{e=(i,j)\in w} \{f_{ij}^+\}. \tag{4.35}$$

We call such an edge (b_1, b_2) a bottleneck.

Here and in the following we somewhat misuse our notation by writing $e = (i, j) \in w$ whenever the edge e is involved in the pathway $w = (i_0, i_1, \ldots, i_n)$, i.e. if there is an $m \in \{0, \ldots, n-1\}$ such that $(i, j) = (i_m, i_{m+1})$.

Now it is straightforward to characterize the "best" reaction pathway, namely, that is the one with the *maximal min-current*.

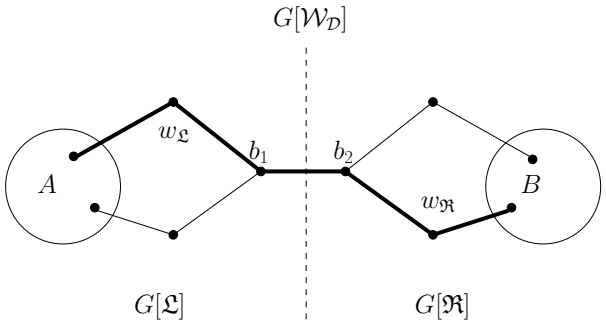

Figure 4.2.: Schematic representation of the decomposition of $\mathcal{W}_\mathcal{D}$. A reaction pathway w (shown in thick black) can be decomposed into two simple pathways $w_\mathfrak{L}$ and $w_\mathfrak{R}$.

Remark 4.1.17. *Notice that the problem of finding a pathway which maximizes the minimal current is known as the* maximum capacity augmenting path problem *[1] in the context of solving the maximal flow problem in a network.*

In general, one cannot expect to find a unique "best" reaction pathway because the bottleneck corresponding to the maximal min-current could be the bottleneck of other reaction pathways too.

Definition 4.1.18. *Let* $\mathbf{W}$ *be the set of all reaction pathways and denote the maximal min-current by* c_{max}*. Then we define the set of the* dominant reaction pathways $\mathcal{W}_\mathcal{D} \subset \mathbf{W}$ *by*

$$\mathcal{W}_\mathcal{D} = \{w \in \mathbf{W} : c(w) = c_{max}\}.$$

Remark 4.1.19. *To guarantee uniqueness of the bottleneck, we henceforth assume that the positive currents of the effective current* f^+ *are pairwise different, i.e.* $f_e^+ \neq f_{e'}^+$ *for all pairs of edges* $e = (i,j), e' = (i',j')$*. Nevertheless, we are aware that in applications the situation could show up where more than one bottleneck exists because the corresponding currents are more or less equal. This ambiguity is taken into account in an hierarchical decomposition of the set of all reaction pathways described at the end of this section.*

Let $G[\mathcal{W}_\mathcal{D}] = G(S_\mathcal{D}, E_\mathcal{D})$ be the directed graph induced by the set $\mathcal{W}_\mathcal{D}$, i.e., the graph whose vertex/edge set is composed of all vertices/edges that appear in at least one of the pathways in $\mathcal{W}_\mathcal{D}$. The next Lemma shows that the graph $G[\mathcal{W}_\mathcal{D}] = G(S_\mathcal{D}, E_\mathcal{D})$ possesses a special structure which is crucial for the definition of a *representative dominant reaction pathway.*

Lemma 4.1.20. *Let* $b = (b_1, b_2)$ *denote the unique bottleneck in* $G[\mathcal{W}_\mathcal{D}]$*. Then the graph* $G(S_\mathcal{D}, E_\mathcal{D} \setminus \{b\})$ *decomposes into two disconnected parts* $G[\mathfrak{L}]$ *and* $G[\mathfrak{R}]$ *such that every reaction pathway* $w \in \mathcal{W}_\mathcal{D}$ *can be decomposed into two pathways* $w_\mathfrak{L}$ *and* $w_\mathfrak{R}$

$$w = (\underbrace{i_{l_1}, \ldots, i_{l_n} = b_1}_{=w_\mathfrak{L}}, \underbrace{b_2 = i_{r_1}, \ldots, i_{r_m}}_{=w_\mathfrak{R}}),$$

where $w_\mathfrak{L} \in \mathfrak{L}$ *is a simple pathway in* $G[\mathfrak{L}]$ *starting in* $i_{l_1} \in A$ *and ending in* $\{b_1\}$ *and* $w_\mathfrak{R}$ *is a simple pathway in* $G[\mathfrak{R}]$ *starting in* $\{b_2\}$ *and ending up in* $i_{r_m} \in B$*. Whenever we have* $\mathfrak{L} = \emptyset$ *then* $G[\mathfrak{L}] = (\{i_{l_1}\}, \emptyset)$*; for* $\mathfrak{R} = \emptyset$ *likewise.*

Here and in the following we write $w_{\mathfrak{L}} \in \mathfrak{L}$ (and $w_{\mathfrak{R}} \in \mathfrak{R}$, respectively) if we want to express that for every edge $e \in w_{\mathfrak{L}}$ we have $e \in \mathfrak{L}$.

Proof. It immediately follows from the definition of $\mathcal{W}_{\mathcal{D}}$ that the bottleneck b is involved in every dominant reaction pathway because otherwise there would exist a pathway $w \in \mathcal{W}_{\mathcal{D}}$ such that $c(w) > c_{max}$ which leads to a contradiction. By definition, a reaction pathway does not possess any loops. Consequently, the bottleneck b separates $\mathcal{W}_{\mathcal{D}}$ which proofs the assertion. □

According to the Lemma, the set of dominant reaction pathways $\mathcal{W}_{\mathcal{D}}$ can be represented as

$$\mathcal{W}_{\mathcal{D}} = \mathfrak{L} \times \mathfrak{R} := \{(w_{\mathfrak{L}}, w_{\mathfrak{R}}) : w_{\mathfrak{L}} \in \mathfrak{L}, w_{\mathfrak{R}} \in \mathfrak{R}\}\,. \tag{4.36}$$

In Figure 4.2 we give a schematic representation of the decomposition of $\mathcal{W}_{\mathcal{D}}$.

Next, we address the most likely case in applications where more than one dominant reaction pathway exists. By definition, each dominant reaction pathway conducts the same amount of current from A to B but they differ with respect to the maximal amount of current which they conduct, e.g., from the set A to the bottleneck, respectively. Now observe that the simple pathways in the set $\mathfrak{L}$ could be seen as reaction pathways with respect to the set A and the B-set $\{b_1\}$. Hence, $\mathfrak{L}$ possesses itself again a set of dominant reaction pathways $\mathcal{W}_{\mathcal{D}}(\mathfrak{L})$ and so on. This motivates the following recursive definition of the a *representative* dominant reaction pathway.

Definition 4.1.21. *Let $\mathcal{W}_{\mathcal{D}} = \mathfrak{L} \times \mathfrak{R}$ and suppose $b = (b_1, b_2)$ is its (unique) bottleneck. Then we define the* representative *dominant reaction pathway w^* of $\mathcal{W}_{\mathcal{D}}$ by*

$$w^* = (w^*_{\mathfrak{L}}, w^*_{\mathfrak{R}}), \tag{4.37}$$

where $w^*_{\mathfrak{L}}$ is the representative dominant pathway of the set $\mathcal{W}_{\mathcal{D}}(\mathfrak{L})$ with respect to the set A and the B-set $\{b_1\}$ and $w^*_{\mathfrak{R}}$ is the representative of $\mathcal{W}_{\mathcal{D}}(\mathfrak{R})$ with respect to the A-set $\{b_2\}$ and the set B. If $\mathfrak{L} = \emptyset$ and $G[\mathfrak{L}] = (\{i\}, \emptyset)$ then $w^*_{\mathfrak{L}} = \{i\}$; if $\mathfrak{R} = \emptyset$ then $w^*_{\mathfrak{R}}$ is defined likewise.

Notice that the representative w^* is unique under the assumption made in Remark 4.1.19. Furthermore, it follows immediately from the recursive definition of w^* that

$$\begin{aligned} w^* =& \arg \max_{w \in \mathcal{W}_{\mathcal{D}}} \min_{\substack{e=(i,j)\in w,\\ (i,j)\neq(b_1,b_2)}} \{f^+_{ij}\} \\ =& \arg \max_{w \in \mathcal{W}_{\mathcal{D}}} \min_{\substack{e=(i,j)\in w,\\ (i,j)\neq(b_1,b_2)}} \{f^+_{ij} - c_{max}\}. \end{aligned} \tag{4.38}$$

Finally, we turn our attention to the *residuum current* which results from updating the effective current of each edge along the representative pathway $w^*_1 = w^*$ by subtracting the min-current $c^{(1)}_{max} = c_{max}$. That is, the residuum current is defined as

$$f^{r,1}_{ij} = \begin{cases} f^+_{ij} - c^{(1)}_{max}, & \text{if } (i,j) \in w^*_1 \\ f^+_{ij}, & \text{otherwise.} \end{cases} \tag{4.39}$$

The graph $G_1 = G\{f_{ij}^{r,1}\}$ induced by the residuum current satisfies the current conservation property in analogy to (4.21). It possesses again a bottleneck, say $\tilde{b}$, a set of dominant pathways and a representative pathway, say w_2^*. If we denote the min-current of w_2^* with respect to the residuum current by $c_{max}^{(2)}$ then it should be clear that $c_{max} = c_{max}^{(1)} > c_{max}^{(2)}$ holds. The property (4.38) of w_1^* guarantees that $c_{max}^{(2)}$ is maximal with respect to all possible residuum currents. We can obviously repeat this procedure by introducing the residuum current $f_{ij}^{r,2}$ by subtracting $c_{max}^{(2)}$ from $f_{ij}^{r,1}$ along the edges belonging to w_2^*, and so on. The resulting iteration terminates when the resulting induced graph $G_{M+1} = G\{f_{ij}^{r,M+1}\}$ no longer contains reaction pathways and leads to a hierarchical enumeration $(w_1^*, w_2^*, \ldots, w_M^*)$ of the set $\mathbf{W}$ of all reaction pathways such that

$$\begin{aligned} &c_{max}^{(i)} > c_{max}^{(j)}, \quad 0 \leq i < j \leq M, \\ &\sum_{i=1}^{M} c_{max}^{(i)} = k_{AB}, \end{aligned} \tag{4.40}$$

where the last identity simply follows from the following equation for the rates $k_{AB}(G_i)$ associated with the graphs $G_1, \ldots, G_M$:

$$k_{AB}(G_i) = k_{AB}(G_{i-1}) - c_{max}^{(i)},$$

where G_0 denotes the original graph $G\{f_{ij}^+\}$, and $k_{AB}(G_{M+1}) = 0$.

Remark 4.1.22. *The composition of the total rate into fraction coming from currents along reactive pathways is a quite general concept in graph theory. We herein just presented a specification of it. We refer the interested reader to, e.g. [1], Section 3.5.*

4.1.9. Relation with Laplacian Eigenmaps and Diffusion Maps

Let us briefly comment about the relevance of our results in the context of data analysis (in particular data segmentation and embedding, i.e., low dimensional representation). Recently, two classes of methods have been introduced to this aim: Laplacian eigenmaps [84, 62, 78, 6, 26] and diffusion maps [16, 55]. The idea behind these approaches is quite simple. Given a set of data points, say $S = \{x_1, x_2, \ldots, x_n\}$, one associates a weight induced graph with weight function $w(x, y)$. This graph is constructed locally, e.g. by connecting all points with equal weights that are below a cut-off distance from each other. These weights are then renormalized by the degree of each node, which means that $w(x, y)$ can be re-interpreted as the stochastic matrix of a continuous Markov chain. Alternatively, it is also possible to interpret the weights as rates and thereby build the generator of a continuous-time Markov chain. In both cases, the properties of the chain are then investigated via spectral analysis of the stochastic matrix or the generator. In particular, the first N eigenvectors with leading eigenvalues, say, $\phi_j(x)$, $j = 1, \ldots, N$ can be used to embed the chain into $\mathbb{R}^N$ via: $x \mapsto (\phi_1(x), \ldots, \phi_N(x))$. The eigenvectors can also be used to segment the original data set into important components (segmentation).

As explained in the introduction, the spectral approach is particularly relevant if the Markov chain displays metastability, i.e. if their exists one or more clusters

of eigenvalues which are either very close to 1 (in the case of discrete-time Markov chains) or 0 (in the case of continuous-time Markov chains). When the chain is not metastable, however, the meaning of the first few eigenvectors is less clear, which makes the spectral approach less appealing. In these situations, TPT may provide an interesting alternative. For instance, if several points (or groups of points) with some specific properties can be singled out in the data set, by analyzing the reaction between pairs of such groups, one will disclose global information about the data set (for instance, the committor functions between these pairs may be used for embedding instead of the eigenvectors). The current of reactive trajectories and dominant reaction pathways will also provide additional information about the global structure of the data set which are not considered in the spectral approach.

4.2. Algorithmic Aspects

In this section we explain the algorithmic details for the computation of the various quantities in TPT. Given the generator L and the two sets A and B, the stationary distribution $\pi = (\pi_i)_{i\in S}$ is computed by solving $\pi^T L = 0$, whereas the discrete forward and backward committors, $q^+ = (q_i^+)_{i\in S}$ and $q^- = (q_i^-)_{i\in S}$, are computed by solving (4.11) and (4.15). Solving these equations numerically can be done using any standard linear algebra package. These objects allow one to compute the probability distribution of reactive trajectories $m^R = (m_i^R)_{i\in S}$ in (4.6), its normalized version $m^{AB} = (m_i^{AB})_{i\in S}$ in (4.8), the probability current of reactive trajectories $f^{AB} = (f_{ij}^{AB})_{i,j\in S}$ in (4.19), and the effective current $f^+ = (f_{ij}^+)_{i,j\in S}$ in (4.28). This also gives the reaction rate k_{AB} via (4.25) or (4.27). Next we focus on the computation of the bottlenecks and representative dominant reaction pathways which is less standard.

4.2.1. Computation of Dynamical Bottlenecks and Representative Dominant Reaction Pathways

From the definition in (4.35) of the bottleneck $b = (b_1, b_2)$ associated with the set of dominant reaction pathways $\mathcal{W}_\mathcal{D}$, it follows that

$$f_e^+ > f_b^+, \quad \forall e \in E_\mathcal{D},\ e \neq b,$$

where $f^+ = (f_{ij}^+)_{i,j\in S}$ is the effective current and $E_\mathcal{D}$ is the edge set of the induced graph $G = G[\mathcal{W}_\mathcal{D}]$. This observation leads to a characterization of the bottleneck which is algorithmically more convenient. Let $E_{sort} = (e_1, e_2, \ldots, e_{|E|})$ be an enumeration of the set of edges of $G = G\{f^+\}$ sorted in ascending order according to their effective current. Then the edge $b = e_m$ in E_{sort} is the bottleneck if and only if the graph $G(S, \{e_m, \ldots, e_{|E|}\})$ contains a reaction pathway but the graph $G(S, \{e_{m+1}, \ldots, e_{|E|}\})$ does not. The bisection-algorithm stated in Algorithm 1 is a direct consequence of this alternative characterization of the bottleneck and is related to the *capacity scaling algorithm* ([1], section 7.3) for solving the maximum flow algorithm. For an alternative algorithm in the context of distributed computing which is based on a modified Dijkstra algorithm see [43].

We also have:

Algorithm 1 Computation of the bottleneck

Input: Graph $G = G\{f^+\}$.
Output: Bottleneck $b = (b_1, b_2)$.
(1) Sort edges of G according to their weights in ascending order
$\Longrightarrow E_{sort} = (e_1, e_2, \ldots, e_{|E|})$.
(2) **IF** the edge $e_{|E|}$ connects A and B **THEN RETURN** bottleneck $b := e_{|E|}$.
(3) Initialize $l := 1$,$r := |E|$.
(4) **WHILE** $r - l > 1$
(5) Set $m := \lfloor \frac{r-l}{2} \rfloor$, $E'(m) := \{e_m, \ldots, e_{|E|}\}$.
(6) **IF** there exists an reaction pathway in $G(S, E'(m))$
(7) **THEN** $l := m$ **ELSE** $r := m$.
(8) **ENDWHILE**
(9) **RETURN** bottleneck $b := e_l$.

Lemma 4.2.1. *The computational cost of Algorithm 1 in the worst case is* $\mathcal{O}(n \log n)$ *where* $n = |E|$ *denotes the number of edges of the graph* $G = G\{f^+\}$.

Proof. Assume that $n = 2^k, k > 1$. First notice that the sorting of the edges of $G = G\{f^+\}$ can be performed in $\mathcal{O}(n \log n)$. In the worst case scenario, the edge $e_1 \in E_{Sort}$ is the bottleneck.[1] When this is the case, the number of edges in the j^{th} repetition of the while-loop would be

$$\frac{n}{2^j},$$

and we would have $k-1$ repetitions. The cheapest way to determine whether there exists an reactive trajectory is to perform a breadth-first search starting in A; the computational cost of that step depends only linearly on the number of edges to be considered, such that we deduce for the worst case effort $T(n)$ of the entire procedure

$$\begin{aligned} T(n) &= \mathcal{O}(kn) + \mathcal{O}(\frac{n}{2}) + \mathcal{O}(\frac{n}{4}) + \ldots + \mathcal{O}(\frac{n}{2^{k-1}}) \\ &= \mathcal{O}\Big(kn + n(\frac{1}{2} + \frac{1}{4} + \ldots + \frac{1}{2^{k-1}})\Big) \\ &= \mathcal{O}(kn) \end{aligned}$$

which by noting that $k = log(n)$ ends the proof. □

The algorithm for computing the unique representative pathway w^* of the set of dominant reaction pathways is a direct implementation of the recursive definition of w^* given in (4.37). Recalling that $\mathcal{W}_{\mathcal{D}}$ can be decomposed as stated in (4.36) and assuming that f^+ takes different values for every edge (i, j), we end up with the Algorithm 2. A rough estimation of the computational cost of this algorithm is $\mathcal{O}(mn \log n)$ where m is the number of edges of the resulting representative pathway w^* and $n = |E|$.

[1] We are aware that the edge e_1 could never be the bottleneck unless all effective currents are equal which is by Remark 4.1.19 excluded. Nevertheless, the following reasoning with respect to e_1 leads only to a slight over-estimation of the computational cost.

Algorithm 2 Representative Pathways

Input: Graph $G = G\{f^+\}$, set A, set B.

Output: Representative $w^* = (w^*_{\mathfrak{L}}, w^*_{\mathfrak{R}})$ of $\mathcal{W}_{\mathcal{D}}(G)$.

(1) Determine bottleneck $b = (b_1, b_2)$ in G via Algorithm 1.

(2) Determine all edges E_{AB} of dominant reaction pathways in G.

(3) Set $w^*_{\mathfrak{L}} := \begin{cases} b_1, & \text{if } b_1 \in A \\ \text{result of the recursion with } (G[E_{AB}], A, \{b_1\}), & \text{if } b_1 \notin A. \end{cases}$

(4) Set $w^*_{\mathfrak{R}} := \begin{cases} b_2, & \text{if } b_2 \in B \\ \text{result of the recursion with } (G[E_{AB}], \{b_2\}, B), & \text{if } b_2 \notin B. \end{cases}$

(5) **RETURN** $(w^*_{\mathfrak{L}}, w^*_{\mathfrak{R}})$

4.3. Illustrative Examples

In this section we illustrate the discrete transition path theory on three examples. The first is the discrete equivalent of a diffusion process in the three-hole potential, which we chose because the results of discrete TPT can directly be compared with the results in Section 3.7.1. This example also establishes a link to the case of continuous state space. The second example deals with a problem from molecular dynamics, the glycine-molecule, and shows that TPT allows to characterize reaction pathways between molecular conformations. In this example we follow two different approaches: In the first approach the dynamics of glycine is given by an incomplete observation of the system in a certain time interval, meaning that we have to deal with the issue of reconstructing the generator of the process given the time series. In the second approach we utilize a discrete analog of diffusion in a free energy landscape to approximate the effective dynamics of glycine in the torsion angle space. The third example arise from the modeling of a genetic toggle switch in chemical kinetics.

4.3.1. Discrete Analog of a Diffusion in a Potential Landscape

In Chapter 3, TPT for diffusion processes was illustrated on the example of a particle whose dynamics is governed by the Smoluchowski dynamics

$$\begin{cases} \mathrm{d}x(t) = -\dfrac{\partial V(x(t), y(t))}{\partial x}\mathrm{d}t + \sqrt{2\beta^{-1}}\,\mathrm{d}W_x(t) \\ \mathrm{d}y(t) = -\dfrac{\partial V(x(t), y(t))}{\partial y}\mathrm{d}t + \sqrt{2\beta^{-1}}\,\mathrm{d}W_y(t), \end{cases} \tag{4.41}$$

where $(x(t), y(t)) \in \mathbb{R}^2$ denotes the position of the particle, $V(x, y)$ is the potential, and the remaining parameters are as in (3.22).

For $V(x, y)$ we chose again the three-hole potential

$$\begin{aligned} V(x,y) = {} & 3e^{-x^2-(y-\frac{1}{3})^2} - 3e^{-x^2-(y-\frac{5}{3})^2} \\ & - 5e^{-(x-1)^2-y^2} - 5e^{-(x+1)^2-y^2} \\ & + \frac{2}{10}x^4 + \frac{2}{10}(y-\tfrac{1}{3})^4 \end{aligned} \tag{4.42}$$

which has been already considered in Section 3.7.1. As one can see in Figure 4.3 the potential (4.42) has two deep minima approximately at $(\pm 1, 0)$, a shallow minimum approximately at $(0, 1.5)$, three saddle points approximately at $(\pm 0.6, 1.1), (-1.4, 0)$ and a maximum at $(0, 0.5)$. As already mentioned, the process defined by (4.42) is ergodic with respect to the invariant measure

$$\mathrm{d}\mu(x, y) = Z^{-1} \exp\left(-\beta V(x, y)\right) \mathrm{d}x \mathrm{d}y, \tag{4.43}$$

where $Z = \int_{\mathbb{R}^2} \exp\left(-\beta V(x, y)\right) \mathrm{d}x\, \mathrm{d}y$ is a normalization constant. If β is small enough, the measure is strongly peaked on the deep minima of the potential (see the left panel of Figure 4.4), and the system displays metastability, i.e. the particle makes transitions between the vicinity of these minima only very rarely. In it was shown that TPT can be used to describe the mechanism of the transition and compute their rates. In particular, it was shown that transitions preferably occur by the upper channel visible in Figure 4.3 when β is very small, but that they proceed by the lower channel when β is somewhat increased. The reasons for this entropic switch were elucidated in Section 3.7.1 and we refer the reader to this section for details. Our purpose here is to apply TPT on a discrete analog of (4.41).

In order to construct this analog, we exploit the well-known fact that a diffusion process can be approximated by a Markov jump process after discretization of state space. For details on the derivation of the generator, given in (4.44), see Section A.3 in the Appendix. Here we approximate the dynamics (4.41) on a two dimensional, rectangular domain $\Omega = [a, b] \times [c, d] \subset \mathbb{R}^2$ via a Birth-Death process on the discrete state space (mesh) $S = (a + h\mathbb{Z} \times b + h\mathbb{Z}) \cap ([a, b] \times [c, d])$ where the mesh width $h > 0$ is chosen such that the corners of Ω are covered by the mesh S. The generator is given by

$$\begin{aligned}(Lf)(x, y) = \quad & k_x^+(x + h, y)(f(x + h, y) - f(x, y)) \\ & + k_x^-(x - h, y)(f(x - h, y) - f(x, y)) \\ & + k_y^+(x, y + h)(f(x, y + h) - f(x, y)) \\ & + k_y^-(x, y - h)(f(x, y - h) - f(x, y)),\end{aligned} \tag{4.44}$$

where

$$k_x^+(x + h, y) = \begin{cases} \dfrac{\beta^{-1}}{h^2} - \dfrac{1}{2h}\dfrac{\partial V(x, y)}{\partial x}, & \text{if } x \in (a, b) \cap (a + h\mathbb{Z}) \\ 0, & \text{if } x = b \\ \dfrac{1}{h}, & \text{if } x = a \end{cases}$$

$$k_x^-(x - h, y) = \begin{cases} \dfrac{\beta^{-1}}{h^2} + \dfrac{1}{2h}\dfrac{\partial V(x, y)}{\partial x}, & \text{if } x \in (a, b) \cap (a + h\mathbb{Z}) \\ 0, & \text{if } x = a \\ \dfrac{1}{h}, & \text{if } x = b \end{cases}$$

and the coefficients k_y^+ and k_y^- are defined analogously with respect to $\partial V(x, y)/\partial y$. In the left panel of Figure 4.4 we show the level sets of the density function $\exp(-\beta V(x, y))$ associated with the Gibbs measure (4.43). In the right panel of Figure 4.4 we illustrate the stationary distribution $\pi = (\pi_i)_{i \in S}$ of the Birth-Death process as a *box plot*.

We now present the results of TPT on this example. The panels in Figure 4.5

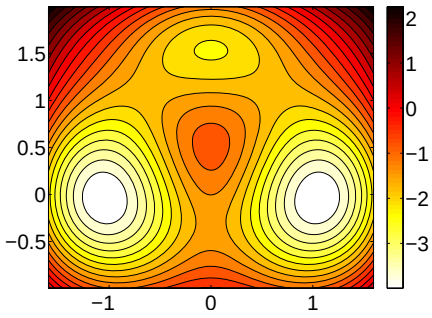

Figure 4.3.: The figure shows the level sets of the three-hole potential given in (4.42). In principal, the dynamics can make a transition between the two main minima via the direct lower channel or via the upper channel through the shallow minima.

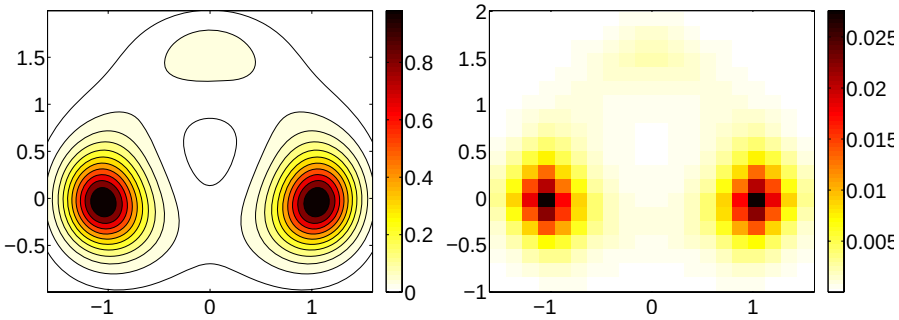

Figure 4.4.: Left: Contour plot of the equilibrium density function $\exp(-\beta V(x))$. Right: Box-plot of the stationary distribution $(\pi_i)_{i\in S}$. Results for $\beta = 1.67$ and a 20×20 mesh discretization.

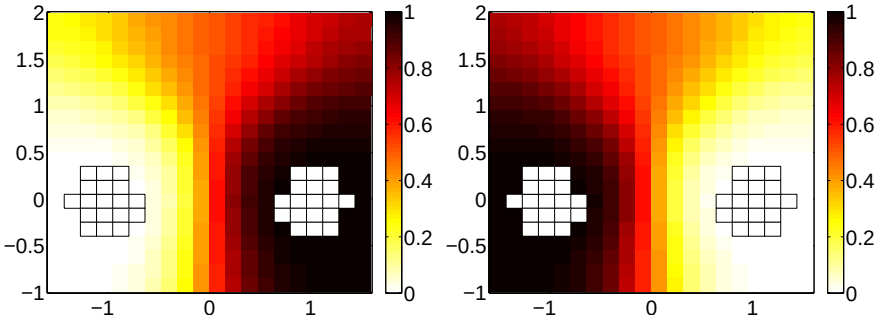

Figure 4.5.: Box-plot of the discrete committors. Left: Forward committor q^+. Right: Backward committor q^-. Results for $\beta = 1.67$ and a 20×20 mesh discretization.

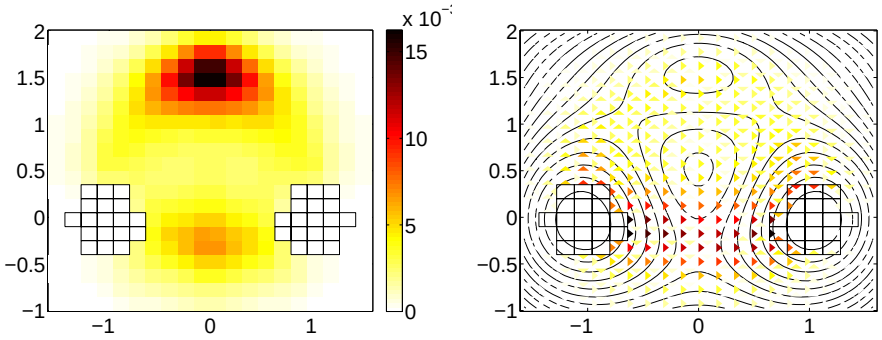

Figure 4.6.: Left: Box-plot of the discrete probability distribution of reactive trajectories m^{AB}. Right: Visualization of the effective current f^+ between mesh points (boxes). An edge (i, j) with positive effective current f_{ij}^+ is depicted by a triangle pointing from the box which corresponds to the state i towards the box identified with $j \in S$. The darker the color of a triangle, the higher the effective current is.

show the box plots of the forward committor q^+ (left panel) and the backward committor q^- (right panel). The set $A \subset S$ is chosen such that it sufficiently covers the region around the left minimum. The set B is defined analogously for the right minimum. The symmetry of the potential together with the symmetry of the sets A and B implies that the particular $\frac{1}{2}$-committor surface, defined as the set $\{i \in S : q_i^+ = 0.5\}$, should correspond to the symmetry axis in y-direction, which is confirmed in Figure 4.5. Notice how the presence of the shallow minima in the upper part of the potential spreads the "level sets" of q^+ in this region. This follows from the fact that the reactive trajectories going through the upper channel get trapped in the shallow well for a long period of time before exiting towards the set B. Next, we turn our attention to the probability distribution of the reactive trajectories, shown in the left panel of Figure 4.6. One can see that the distribution has a peak in the upper shallow minima whereas the effective current, visualized in the right panel of Figure 4.6, suggests that most of the reactive trajectories prefer the lower channel. This again can be explained by the fact that the reactive trajectories going through the upper channel get trapped in the shallow well whereas the reactive trajectories in the lower channel just need to overcome the barrier. We end this example by discussing the family of dominant reaction pathways resulting from the procedure described in the end of Section 4.2.1. In Figure 4.7 we plot the family of reaction pathways which covers about 50% of the probability flux of reactive trajectories for two different temperature, respectively. The pathways are colored according to the values of their min-currents. The darker the color, the larger the current conducted by the corresponding reaction pathway is. At the high temperature ($\beta = 1.67$, left panel), the reaction happens mostly via the lower channel, whereas at low temperature ($\beta = 6.67$, right panel) it occurs mostly via the upper channel. This is consistent with the results presented in [73] and in Section 3.7.1. Finally, we present in Figure 4.8 the family of dominant reaction pathways in the perturbed three-hole potential which has already been considered in Section 3.7.1. We used the same perturbation of three-hole potential as well as the same (discrete) sets A and B as for the smooth three-hole potential above. As one can see, the

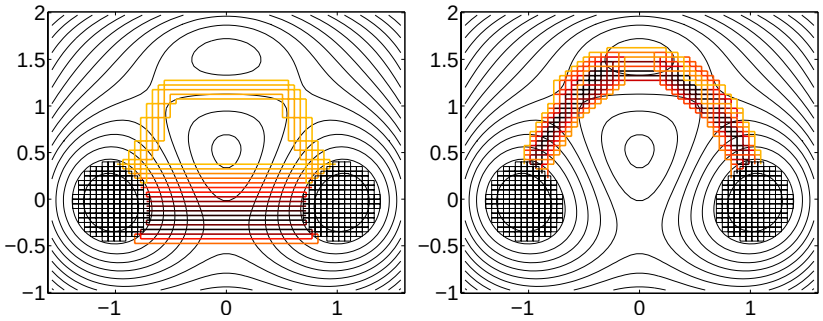

Figure 4.7.: Reaction pathway families for two different temperatures. Both families cover about 50% of the probability flux of reactive trajectories, respectively. The pathways are colored according to the values of their min-currents. The darker the color the more current is conducted by the corresponding reaction pathway. Left: Reaction pathway family at a high temperature $\beta = 1.67$. Right: Reaction pathway family at a low temperature $\beta = 6.67$. Results for a 60×60 mesh discretization; for the sake of illustration the mesh is chosen finer than before.

transition behavior described in Section 3.7.1 is recovered by the discrete TPT.

4.3.2. Molecular Dynamics : Glycine

In this example we use discrete TPT to study conformation changes of the glycine-molecule which is shown in ball-and-stick representation in the left panel of Figure 4.9. We have seen that the essential object in discrete TPT is the generator of the considered Markov jump process. Unlike in the previous example, here the generator of the process is not directly available. Nevertheless, we will present two approaches both yielding a generator of a Markov jump process which describes the dynamics of glycine in terms of the torsion angles Φ and Ψ at room temperature $300K$.

In the first approach the dynamics of the glycine-molecule in solvent is given by a time series of the two torsion angles Φ and Ψ. The main challenge here was to estimate a generator of a Markov jump process representing the dynamics on a coarse grained state space of the torsion angle space (Φ, Ψ). The details of the estimation procedure are described in Chapter 5. For a more detailed analysis of the conformation see [61]. In the second approach we apply the technique presented in the previous section in order to approximate the dynamics of glycine in an interpolated discrete free energy landscape via a Birth-Death process.

Time Series Approach

The time series used herein was extracted out of a molecular simulation of the glycine-molecule embedded in a cubic box of edge length 3.51 nm with 1402 water molecules. The integration of the trajectory with total length $T = 5$ nanoseconds was realized with $\tau = 2$ fs time steps in the Leapfrog-integration scheme with GROMACS force field [8, 59] at room temperature of 300K. In the right panel of Figure 4.9 we give a snapshot of a trajectory where the glycine-molecule is shown together with

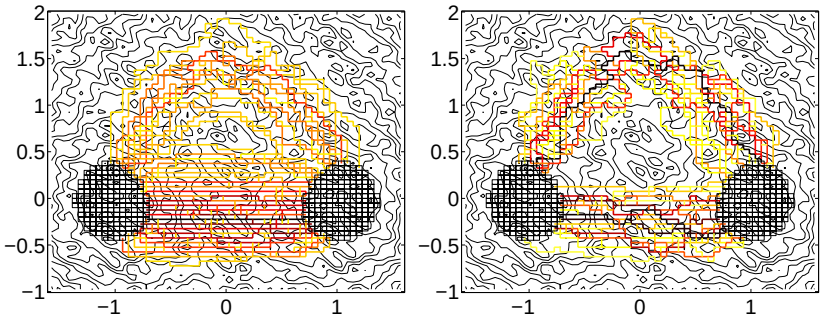

Figure 4.8.: Reaction pathway families in the perturbed three-hole potential in (3.46) at high temperatures $\beta = 1.67$ (left panel) and at low temperature $\beta = 6.67$ (right panel). We used the same perturbation of the potential as in Section 3.7.1. Both families cover about 50% of the probability flux of reactive trajectories, respectively. The pathways are colored according to the values of their min-currents. The darker the color the more current is conducted by the corresponding reaction pathway. Results for a 60×60 mesh discretization.

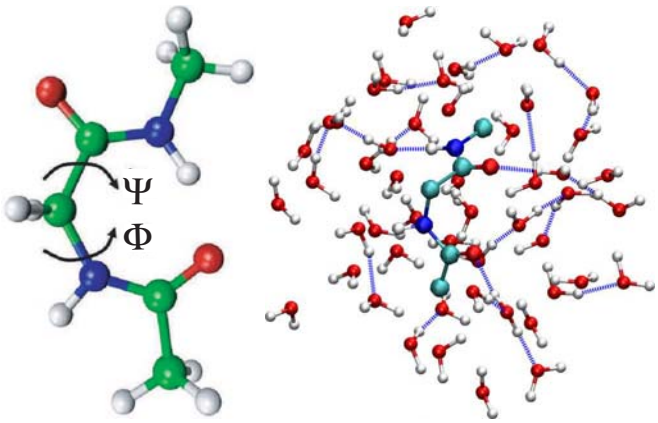

Figure 4.9.: Left: The glycine-molecule shown in ball-and-stick representation and the two torsion angles Φ and Ψ. Right: This panel shows a snapshot of the respective trajectory where the glycine-molecule is shown together with the nearest water molecules.

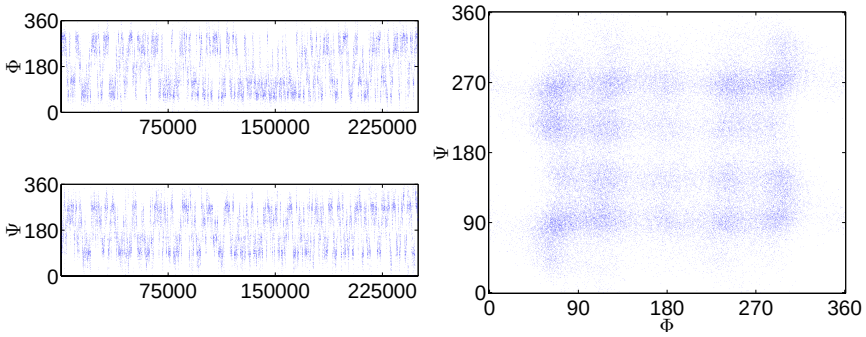

Figure 4.10.: Left: Projection of the time series (all atomic positions) onto the torsion angle space spanned by Φ and Ψ. Right: The Ramachandran plot of the time series in the torsion angle space (Φ, Ψ) reveals the metastable behavior of the dynamics. At first glance, the molecule attains four main conformations where each conformation could be decomposed further into four conformations. We will focus, however, on the four main conformations.

the nearest water molecules. In order to ensure the Markov property later on, we considered only every 100^{th} step of the original trajectory. Before explaining how we constructed a Markov jump process with discrete state space (and especially its generator) out of this time series, let us give some background about this example.

Metastability and Conformation states A conformation of a molecule is understood as a mean geometric structure of the molecule which is conserved on a large time scale compared to the fastest molecular motions. From the dynamical point of view, a conformation typically persists for a long time (again compared to the fastest molecular motions) such that the associated subset of configurations is *metastable* [82]. In the left panel of Figure 4.10 we show the projection of the time series of the torsion angles Φ and Ψ which clearly reveals the metastable behavior. The Ramachandran plot of the time series in the right panel of Figure 4.10 illustrates the dependency of the conformation states on the two torsion angles. At first glance, the molecule attains four main conformations in the torsion angle space.

Generator Estimation The first step towards the application of discrete TPT is to determine a coarse grained model of the dynamics in the torsion angle space based on the given time series. We discretized the two-dimensional torsion angle space with a 20×20 equidistant box discretization and identified each element of the time series with the box by which it is covered. Assuming that the resulting discrete time series is Markovian, we estimated a reversible Markov jump process on the discrete state space of boxes which most likely explains the discrete time series. This is done by using an efficient generalization of the maximum-likelihood method presented in detail in Chapter 5. For details on the estimation of the generator for this example see Section 5.4.5.

In the following, we denote by $\tilde{L}_{MLE} = (\tilde{l}_{ij})_{i,j \in S}$ the infinitesimal generator of the estimated Markov jump process. For the sake of illustration, we show in the left panel

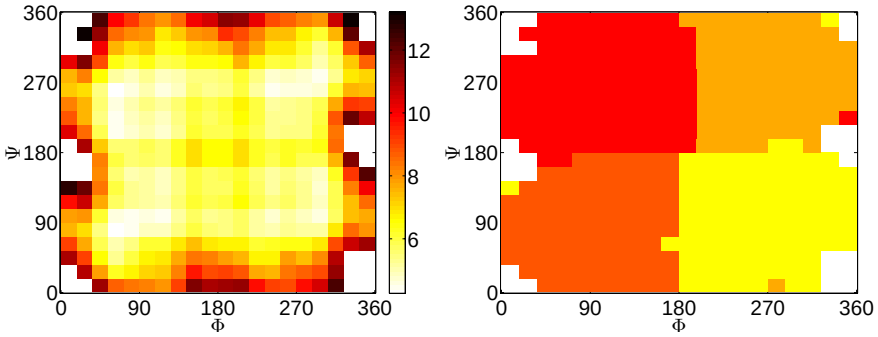

Figure 4.11.: Left: Box plot of the discrete free energy, $-log(\pi_i)$, where $(\pi_i)_{i\in S}$ is the stationary distribution computed from the estimated generator $\tilde{L}_{MLE}$. The lighter the color of a box is the more probable to encounter the equilibrated jump process in the corresponding state. Right: The decomposition of the torsion angle space into four metastable subsets resulting from PCCA .

of Figure 4.11 the *discrete free energy*, $-log\ \pi_i$, where $(\pi_i)_{i\in S}$ is the stationary distribution computed from the estimated generator $\tilde{L}_{MLE}$ with respect to a 20×20 box discretization. The lighter the color of a box is the more probable it is to encounter the equilibrated process in the corresponding state. In order to determine the number of metastable subsets and the subsets itself, we have to look at the dominant eigenvalues of the transition matrix $\tilde{P}(\tau) = \exp(\tau\tilde{L}_{MLE}), \tau = 2 \cdot 10^{-13}$ as listed in Table 5.3 in Section 5.4.5). The gap between the fourth and the fifth dominant eigenvalue suggests a decomposition of the state space (torsion angle space) into four metastable subsets. Algorithmically, the decomposition was performed via the Perron Cluster Cluster Analysis (PCCA) [24, 17]. The symmetry of the resulting four metastable subsets, as illustrated in the left panel of Figure 4.11, shows that the estimated generator captures the dynamics in the coarse grained torsion angle space.

Analysis within Transition Path Theory We were interested in the reaction pathways between two main conformations - the upper left one and the lower right one. As the set B we chose the box in which the discrete free energy restricted on the upper left conformation attains its minimum. The set A was selected analogously with respect to the lower right conformation. The discrete forward committor q^+ is given in the left panel of Figure 4.12. Comparison of the distribution of reactive trajectories m^{AB} (illustrated in the right panel of Figure 4.12) with the family of dominant reaction pathways (right panel of Figure 4.13) reveals again that m^{AB} is insufficient to describe the effective dynamics from A to B. To see this, notice that since we deal with a periodic boundary the distribution of reactive trajectories m^{AB} does not tell anything about the orientation of the direction in which a reaction takes place.

The family of dominant reaction pathways which cover about 20% of the transition rate is given in the left panel of Figure 4.13. The darker the color of a pathway the more current it conducts from A to B. Each of the two darkest reaction pathways

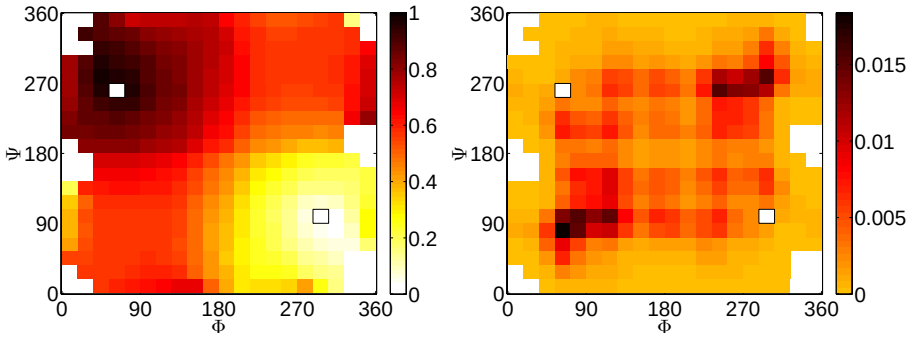

Figure 4.12.: Left: This figure shows the forward committor q^+ computed via (4.11). As the set A we chose the box (shown as a white box with black boundary) which covers the peak of the restricted stationary distribution on the lower right conformation. The set B for the upper left conformation (shown as a white box) was chosen analogously. Right: Box plot of the discrete probability distribution of reactive trajectories m^{AB}.Results are for an equidistant discretization of the torsion angle space into 20×20 boxes.

covers about 6% of the rate which shows that the upper and lower reaction channel are more or less equivalent. That observation is consistent with the symmetry of the glycine-molecule in terms of the considered torsion angles. The family of dominant reaction pathways with respect to 30% of the reaction rate (shown in the right panel of Figure 4.13) reveals that there exists an additional third reaction pathways with an opposite orientation.

Free Energy Landscape Approach

In the timeseries approach we consider the dynamical information (the trajectory) to derive the generator of the underlying process. In the free energy approach we assume that the dynamics of the observables (here the two torsion angles) can be described by a Smoluchowski dynamics in a free energy landscape associated with these observables. For a short account to free energy with respect to Smoluchowski dynamics see Section A.5 in the Appendix.

Suppose that we are given a periodic potential landscape $V(\Phi, \Psi) : [0, 2\pi] \times [0, 2\pi] \to \mathbb{R}$ such that the dynamics in the torsion angles Φ and Ψ is governed by

$$\begin{cases} \mathrm{d}\Phi(t) = -\dfrac{\partial V(\Phi(t), \Psi(t))}{\partial \Phi}\mathrm{d}t + \sqrt{2\beta^{-1}}\,\mathrm{d}W_\Phi(t) \\ \mathrm{d}\Psi(t) = -\dfrac{\partial V(\Phi(t), \Psi(t))}{\partial \Psi}\mathrm{d}t + \sqrt{2\beta^{-1}}\,\mathrm{d}W_\Psi(t). \end{cases} \tag{4.45}$$

Our crucial observation now is that the approach presented on the three-hole example in Section 4.3.1 can straightforwardly be generalized to that situation. The only difference for the approximation of the dynamics in (4.45) via a Birth-Death process is that we have to incorporate *periodic* boundary conditions instead of reflecting boundary conditions. To be more precise, we discretized the square $\Omega =$

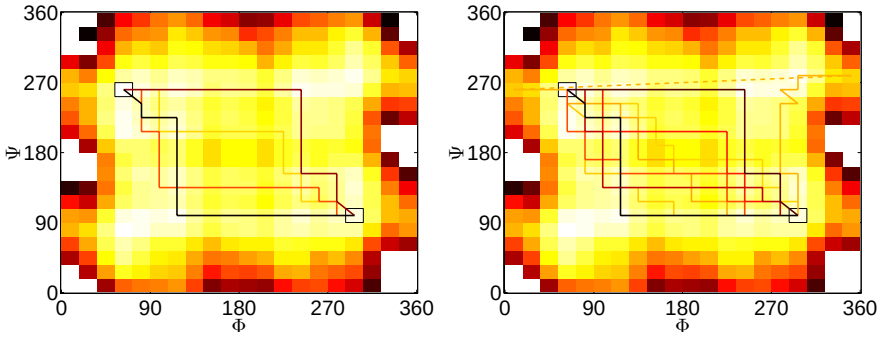

Figure 4.13.: Family of dominant reaction pathways which cover about 20% (left panel) and 30% (right panel) of the reaction rate k_{AB}. The darker the color of a pathway the more current it conducts from A to B. For the sake of illustration, the dominant reaction pathways are embedded in the box plot of the discrete free energy. Each of the two darkest reaction pathways covers about 6% of the rate which shows that the upper and lower reaction channel are more or less equivalent which is consistent with the symmetry of the glycine-molecule. The family shown in the right panel reveals that there exists an additional third reaction pathway, indicated by the long edge in the upper part of the panel.

$[0, 2\pi) \times [0, 2\pi)$ with a total uniform mesh

$$\Omega_h = \{(\Phi_0 + ih, \Psi_0 + jh) : 0 \leq i, j \leq N\}$$

such that

$$\Phi_0 \equiv (\Phi_0 + (N+1)h) \bmod 2\pi \text{ and } \Psi_0 \equiv (\Psi_0 + (N+1)h) \bmod 2\pi.$$

The condition on the boundary mesh points accounts for the periodicity of the torsion angle space. Then the generator L of the Birth-Death process is given by (cf. (4.44) and Sect. A.3))

$$\begin{aligned}(Lf)(\Phi,\Psi) = \quad & k_\Phi^+(\Phi+h,\Psi)(f(\Phi+h,\Psi)-f(\Phi,\Psi)) \\ & + k_\Phi^-(\Phi-h,\Psi)(f(\Phi-h,\Psi)-f(\Phi,\Psi)) \\ & + k_\Psi^+(\Phi,\Psi+h)(f(\Phi,\Psi+h)-f(\Phi,\Psi)) \\ & + k_\Psi^-(\Phi,\Psi-h)(f(\Phi,\Psi-h)-f(\Phi,\Psi)),\end{aligned} \tag{4.46}$$

where

$$\begin{aligned} k_\Phi^+(\Phi+h,\Psi) &= \frac{\beta^{-1}}{h^2} - \frac{1}{2h}\frac{\partial V(\Phi,\Psi)}{\partial \Phi}, \quad \text{if } \Phi \in (0,2\pi) \cap (\Phi_0 + h\mathbb{Z}) \\ k_\Phi^-(\Phi-h,\Psi) &= \frac{\beta^{-1}}{h^2} + \frac{1}{2h}\frac{\partial V(\Phi,\Psi)}{\partial \Phi}, \quad \text{if } \Psi \in (0,2\pi) \cap (\Phi_0 + h\mathbb{Z}) \end{aligned}$$

and the coefficients k_Ψ^+ and k_Ψ^- are defined analogously with respect to $\partial V(\Phi,\Psi)/\partial\Psi$.

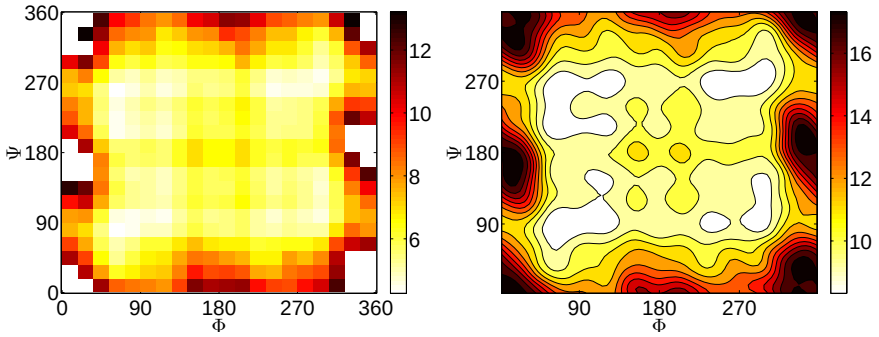

Figure 4.14.: Left: The discrete free energy, $-\log \pi_i$, resulting from the time series approach with respect to the decomposition of the torsion angle space (Φ, Ψ) into 20×20 boxes. Right: The continuous representation of the discrete free energy via a Fourier ansatz.

Analysis within Transition Path Theory Our crucial step towards the comparison of the time series approach with the free energy approach is to interpolate the discrete free energy on a mesh consisting of the box centers of the torsion angle space decomposition.

To be more precise, consider the 20×20 box-decomposition of the torsion angle space (Φ, Ψ) from the analysis of the time series in the previous section. Let $(\Phi_i, \Psi_i),\ i = 1, \ldots, 20^2$ denote the centers of a decomposition boxes. Since the time series does not visit all boxes of the decomposition, the free energy for the empty boxes (depicted as the white regions in left panel of Figure 4.14) is not defined. For the numerical interpolation, however, we set the free energy of not visited boxes to a sufficiently high value such that they result in a barrier for the diffusion dynamics.

Due to the periodicity of the torsion angle space, we can use a Fourier ansatz for the numerical interpolation:

$$V(\Phi_i, \Psi_i) = \pi_i = \sum_{k,l=0}^{M} \big[(a_k \sin(k\Phi_i) + b_k \cos(k\Phi_i))(c_l \sin(l\Psi_i) + d_l \cos(l\Psi_i))\big],$$

where $i = 1, , \ldots, 20^2$ and determine the coefficients $a_k, b_k, c_l, d_l, 0 \leq l, k \leq M$ by means of the least square method. The right panel in Figure 4.14 illustrates the interpolated discrete free energy landscape[2]. For our numerical experiment we set $M = 12$.

The main question is now if the Birth-Death process (given via the construction in (4.46)) in the interpolated landscape exhibits the same transition behavior as detected with the time series approach? To answer this question, we constructed a generator L via (4.46) on a 70×70 (periodic) mesh discretization of the square $[0, 360] \times [0.360]$. The inverse temperature β was set such that it corresponds to room temperature of 300K. As the set A, we chose the set of mesh points which are covered by the single discretization box associated with the reactant state in the time series approach. The B was chosen analogously. The forward committor q^+ and the distribution m^{AB} of reactive trajectories are given in Figure 4.15.

[2]For illustrative convenience, we present the results in a continuous manner (contour plots) rather than using box plots as in the previous sections.

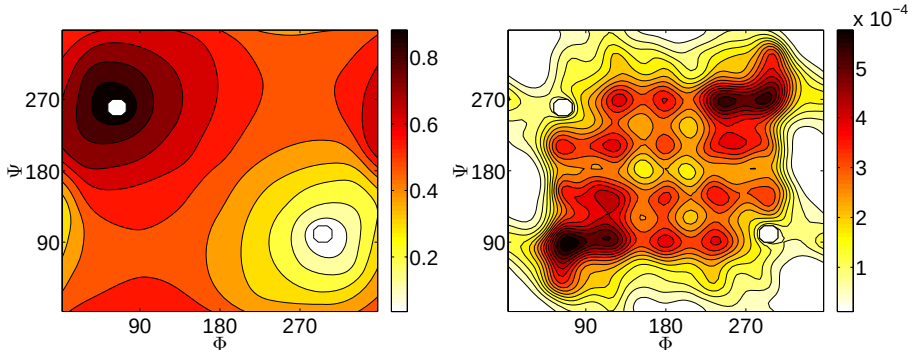

Figure 4.15.: The left panel shows the committor function q^+ with respect to the sets A (bottom right) and B (top left). The distribution m^{AB} is illustrated via a contour plot in the right panel.

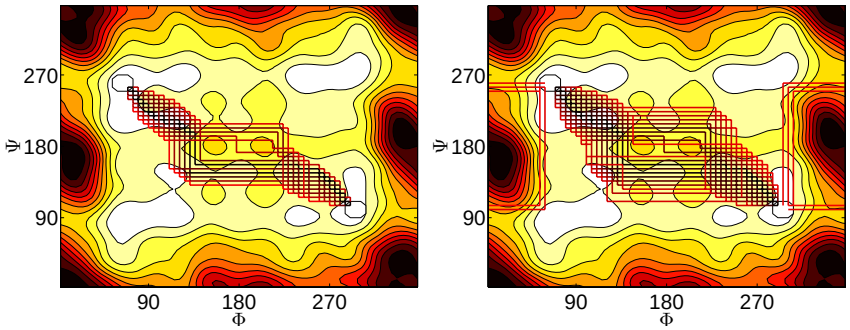

Figure 4.16.: In this figure we illustrate two families of reaction pathways. The family which covers 10% of the transition rate (left panel) reveals that there are two dominant symmetric reaction channels. In the family with respect to 20% (right panel) two additional reaction channels appear but with opposite orientation.

Finally, we present in the panels of Figure 4.16 two families of reaction pathways, one family with respect to 10% (left panel) of the rate k_{AB} and the other family is with respect to 20% (right panel). In comparison to the time series approach, one can see that the symmetry of the two dominant reaction channels is reproduced and more or less their spatial relation to each other (cf. right panel of Figure 4.13). The family with respect to 20% of reaction rate clearly reveals two additional channels where the upper one is consistent with the third channel in the time series approach.

At the end of this example, we want to point out that the (infinitesimal) generator L in (4.46) can also be used to compute the objects of the continuous TPT since L results from the finite differences discretization of the generator $\mathcal{L}_{bw}$ associated with the diffusion process in (4.45). For example, in Figure 4.17 we show the transition tubes resulting from the streamlines associated with the probability current in (3.28) (cf. Sect. 3.1.5). As a dividing surface we chose a circle with radius $r = 1$ around the center of the set A. The resulting tubes are consistent with the reaction pathways found within the discrete setting.

The results of this section have shown that discrete TPT can be used to analyze

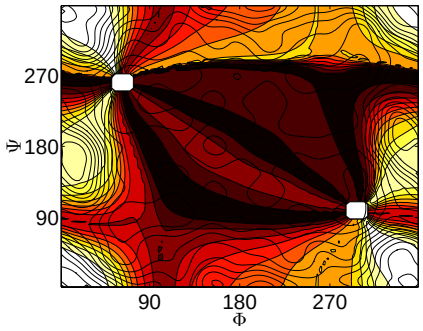

Figure 4.17.: The transition tubes resulting from the streamlines associated with the probability current in (3.28). Results for .

transition events in conformational dynamics. We have presented two different approaches - TPT in combination with the generator estimation and the free energy approach. Both approaches lead to reasonably and comparable results.

4.3.3. Chemical Kinetics

In the last example, we consider a Markov jump process which arises as a stochastic model of a genetic toggle switch consisting of two genes that repress each others' expression [77].

The expression of the each of the two respective genes results in the production of a specific type of protein; gene G_A produces protein P_A and gene G_B protein P_B. Denote the number of available proteins of type P_A by x and of type P_B by y, the model for the toggle switch proposed in [77] is a Birth-Death process on the discrete state space $S = (\mathbb{Z} \times \mathbb{Z}) \cap ([0, d_1] \times [0, d_2]), d_1, d_2 > 0$, whose generator is given by:

$$\begin{aligned}(Lf)(x,y) = c_1(x+1,y)(f(x+1,y) - f(x,y)) \\ + \frac{x}{\tau_1}(f(x-1,y) - f(x,y)) \\ + c_2(x,y+1)(f(x,y+1) - f(x,y)) \\ + \frac{y}{\tau_2}(f(x,y-1) - f(x,y)),\end{aligned} \tag{4.47}$$

where

$$c_1(x+1,y) = \begin{cases} \dfrac{a_1}{1+(y/K_2)^n}, & \text{if } x \in [0, d_1) \\ 0, & \text{if } x = d_1, \end{cases}$$

$$c_2(x,y+1) = \begin{cases} \dfrac{a_2}{1+(x/K_1)^m}, & \text{if } y \in [0, d_2) \\ 0, & \text{if } y = d_2. \end{cases}$$

We refer to [77] for the biological interpretation of the parameters in (4.47). For our numerical experiments, we used the parameters $a_1 = 156, a_2 = 30, n = 3, m = 1, K_1 = K_2 = 1, \tau_1 = \tau_2 = 1$, consistent with [77]. With these parameters the system's dynamical behavior is as follows: There are two "metastable" states; in the first of these only gene G_A is expressed and protein P_A is produced until a certain number (around $x = 155$ for the parameters chosen) is reached which then is rather

stable, while gene G_B is repressed and almost no protein P_B is produced (so that typically $y = 0$ or $y = 1$). After some rather long period of fluctuation in this metastable state the system is able to exit from it which leads to expression of gene G_B and repression of G_A. Then the system gets into a metastable state where the number of protein P_B fluctuates around a certain non-vanishing number ($y = 30$ for our parameters) and P_A is rather not produced (typically $x = 0$ or $x = 1$).

It is well-known that in the limit of large protein numbers the dynamics of the jump process or, more precisely, of the associated Master equation is given by a deterministic model of the biochemical kinetics in terms of the associated concentrations. The authors in [77] also consider this deterministic model in order to get a rough understanding of the switch dynamics. The model consists of two coupled ordinary differential equations,

$$\begin{aligned} \dot{x} &= \frac{a_1}{1 + (y/K_2)^n} - \frac{x}{\tau_1}, \\ \dot{y} &= \frac{a_2}{1 + (x/K_1)^m} - \frac{y}{\tau_2}, \end{aligned} \tag{4.48}$$

where the parameters are the same as in the stochastic model (4.47). For our particular choice of parameters the deterministic dynamics in (4.48) has two stable stationary points approximately at $(x, y) = (155, 0)$ and $(x, y) = (0, 30)$.

For the sake of illustration, we illustrate in the left panel of Figure 4.18 the Gibbs energy, $-\log \pi$, of the Birth-Death process instead of its stationary distribution π itself. Moreover, we neglected all states with almost vanishing stationary distribution (depicted by the white region) and in order to emphasize the states of interest, we chose a log-log representation. The color scheme is chosen such that the darker the color of a region the more probable to find the process there. One can clearly see that the process spends most of its time near the two metastable core sets $(x, y) \in \{(155, 0), (155, 1)\}$ and $(x, y) \in \{(0, 30), (1, 30)\}$.

We were interested in the reaction from the set $A = \{(155, 0), (155, 1)\}$ towards the set $B = \{(0, 30), (1, 30)\}$. The different shapes of the level sets of the discrete forward and backward committor, as shown in the left and right panel of Figure 4.19, indicate the high non-reversibility of the Birth-Death process. Notice that the geometry of the level sets of the forward committor q^+ looks very similar to the geometry of the eigenvector associated with the first non-trivial right eigenvalue of L, as plotted in the right panel of Figure 4.18. Finally, the edges of the three most dominant reaction pathways are plotted in the right panel of Figure 4.20. Again, the reaction pathways deviate from the channel which is suggested by the distribution m^{AB} of reactive trajectories, shown in the left panel of Figure 4.20.

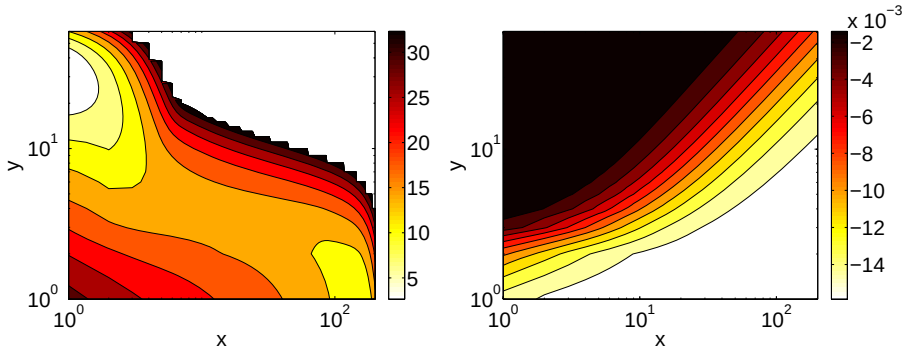

Figure 4.18.: Left: Contour plot of the discrete free energy, $-log\pi_i$, of the Birth-Death process (4.47) on the state space $S = \mathbb{Z} \times \mathbb{Z} \cap ([0, 200] \times [0, 60])$. The white region in the right upper part of the panel indicates the subset of states with almost vanishing stationary distribution (all boxes with distribution less than machine precision have been colored white). Right: Contour plot of the eigenvector of the first non-trivial right eigenvalue of L. Results for $a_1 = 156, a_2 = 30, n = 3, m = 1, K_1 = K_2 = 1, \tau_1 = \tau_2 = 1$.

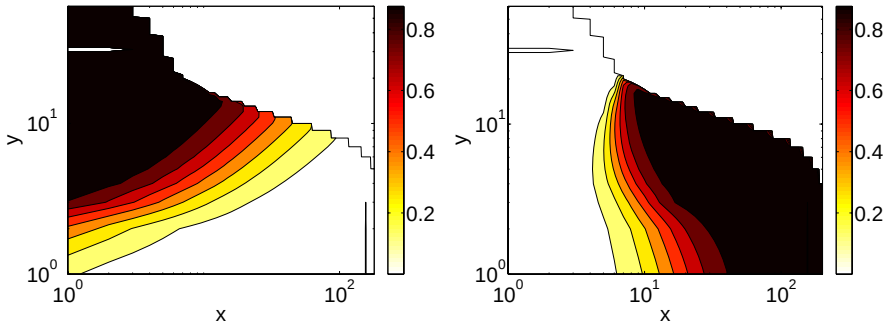

Figure 4.19.: Contour plots of the discrete forward and backward committor. Due to the logarithmic scaling, the set $A = \{(155, 0), (155, 1)\}$ is depicted as a vertical black line and the set $B = \{(0, 30), (1, 30)\}$ as an ellipsoid. Left: Discrete forward committor q^+. Right: Discrete backward committor q^-.

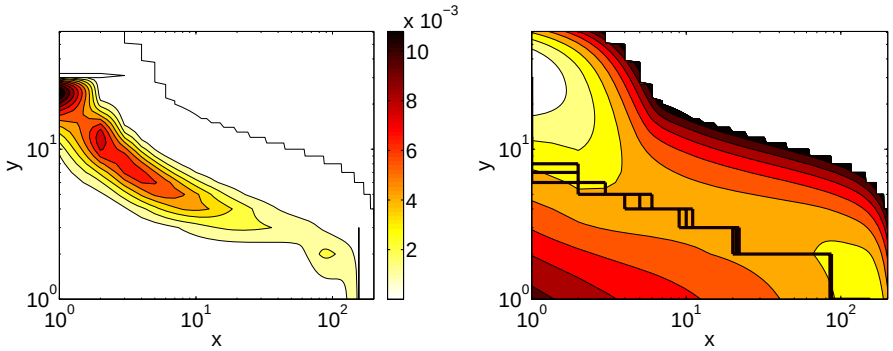

Figure 4.20.: Left: Contour plot of the distribution of reactive trajectories m^{AB}. Right: Edge plot of the three dominant reaction pathways which cover about 6% of the current.